Helmholtz-Zentrum Dresden-Rossendorf (HZDR)

HELMHOLTZ ZENTRUM
DRESDEN ROSSENDORF

Transition from convection rolls to large-scale cellular structures in turbulent Rayleigh-Bénard convection in a liquid metal layer

Akashi, M.; Yanagisawa, T.; Tasaka, Y.; Vogt, T.; Murai, Y.; Eckert, S.;

Originally published:

March 2019

Physical Review Fluids 4(2019)3, 033501

DOI: https://doi.org/10.1103/PhysRevFluids.4.033501

Perma-Link to Publication Repository of HZDR:

https://www.hzdr.de/publications/Publ-28127

Release of the secondary publication
on the basis of the German Copyright Law § 38 Section 4.

Transition from convection rolls to large-scale cellular structures in turbulent Rayleigh–Bénard convection in a liquid metal layer

Megumi Akashi,[1,2] Takatoshi Yanagisawa,[3,1] Yuji Tasaka,[1,*] Tobias Vogt,[2] Yuichi Murai,[1] and Sven Eckert[2]

[1] *Laboratory for Flow Control, Hokkaido University, Sapporo, Japan*
[2] *Helmholtz Zentrum Dresden-Rossendorf (HZDR), Dresden, Germany*
[3] *Japan Agency for Marine-Earth Science and Technology (JAMSTEC), Yokosuka, Japan*

(Dated: July 28, 2018)

Turbulent Rayleigh–Bénard convection was investigated within a liquid metal layer, Prandtl number Pr = 0.03, in a square vessel having a moderate aspect ratio, $\Gamma = 5$. Laboratory experiments were performed at moderate Rayleigh numbers, $7.9 \times 10^3 < \mathrm{Ra} < 3.5 \times 10^5$. Ultrasonic velocity profiling (UVP) was used to visualize the spatio-temporal flow structure in two horizontal planes, while temperature fluctuations were monitored simultaneously in the fluid layer. By using multiple ultrasonic sensors, a grid of orthogonal measurement lines was created. This configuration enabled the identification of coherent flow structures showing periodic oscillations. In particular, oscillatory roll-like structures were observed at $\mathrm{Ra} \geq 10^4$, while the transition to a fully three-dimensional cell-like structure occurs around $\mathrm{Ra} = 6 \times 10^4$. The Fourier analysis of the temperature fluctuations indicates that the convection reaches the developed state of thermal turbulence at this Ra number. The cell-like structure of the flow field is recognized as a representation of the large-scale circulation (LSC) in thermal turbulence for the specific situation of confined convection in the rectangular vessel. The transition from laminar convection to thermal turbulence manifests itself in the occurrence of unstable intermediate regimes accompanied by a stepwise increment in the horizontal scale. We propose a scaling law for the horizontal length scale as a function of Ra based on empirically-derived relations of the oscillation frequency and the typical flow velocity. This scaling law provides an excellent representation also for variations of the maximum size of large-scale circulations in an air layer [T. Hartlep *et al.*, Phys. Rev. Lett. **91**, 064501 (2003) and D. E. Fitzjarrald, J. Fluid Mech. **73**, 693 (1976)], and is supposed to be widely applicable even for higher Pr numbers and different vessel geometries.

I. INTRODUCTION

Rayleigh–Bénard convection (RBC) designates buoyancy driven flows in a fluid layer heated from below and cooled from above. It is a classical problem in fluid dynamics and can be taken as a basic configuration for various issues in geophysics, astrophysics and engineering. The RBC system is dominated by two dimensionless control parameters, the Rayleigh number, $\mathrm{Ra} = \alpha g \Delta T L^3/(\kappa\nu)$, and the Prandtl number, $\mathrm{Pr} = \nu/\kappa$, where α, κ and ν denote the thermal expansion coefficient, the thermal diffusivity, and the kinematic viscosity of test fluids, respectively. The symbols g and ΔT stand for the gravitational acceleration and the vertical temperature difference in the fluid layer with a thickness L. Different convective flow patterns can be found in the Ra – Pr parameter space. Thermal turbulence appears at sufficiently large Ra numbers, while it is widely expected that the flow tends to be more turbulent the smaller the Pr number is (cf. Ref. 1 and 2).

It is well-known that under the condition of thermal turbulence a mean flow is spontaneously formed in a finite convection cell. The existence of such flow structures, termed "large-scale circulation (LSC)", was first reported by Krishnamurti & Howard [2]. The LSC is driven by systematic drift of transient thermal plumes and is therefore not to be confused with the typical convection rolls that form directly after the onset of thermal convection. It is obvious that the structure and the properties of the LSC should depend on both the Ra and the PR number as well as the geometry of the convection cell. The spatio-temporal characteristics of the LSC have been investigated mainly for water ($\mathrm{Pr} \sim 7$) and air ($\mathrm{Pr} \sim 1$) layers (e.g. Ref. 3 and 4). Most of the previous studies are restricted to aspect ratios of the fluid layer (Γ) around unity at which a single roll LSC occupies the entire fluid layer. Only a few examples of thermal turbulence examined in fluid layers with $\Gamma \gg 1$ have been reported yet. From numerical simulations it is reported that the typical size of the LSC in an air layer at $\Gamma = 10$ increases discretely with increasing Ra [5]. Hartlep *et al.* [5] also mentioned that the large-scale structures are continuations of the structures formed in laminar conditions at smaller Ra numbers. von Hardenberg *et al.* [6] performed numerical simulations of convection in air with $2\pi \leq \Gamma \leq 12\pi$ and showed that there is a finite horizontal saturation scale of large scale patterns for sufficiently large Γ in the range, $10^5 \leq \mathrm{Ra} \leq 10^8$. By three-dimensional direct numerical simulation in a shallow cylindrical vessel with $\Gamma \sim 50$, Emran and Schumacher [7] demonstrated that time-averaged streamlines at $\mathrm{Ra} = 5 \times 10^5$ reveal organized convection patterns very similar to those observed at a slightly supercritical Ra number of 5×10^3, while the instantaneous streamlines appear complex and disorganized. Bailon–Cuba *et al.* [8] investigated heat

* tasaka@eng.hokudai.ac.jp

transport and corresponding transitions of flow patterns in thermal turbulence in an air layer as a function of Γ ($0.5 \leq \Gamma \leq 12$); LSC exhibits multiple roll structures or hexagonal cell structures similar to those observed at slightly supercritical conditions close to the onset of convection for sufficiently large aspect ratios ($\Gamma \geq 8$). For lager Ra numbers, $\mathrm{Ra} = 9.6 \times 10^7$, numerical simulations performed by Sakievich *et al.* [9] showed the formation of hub-and-spoke structures as long-living coherent structures in a cylindrical domain at $\Gamma = 6.3$ and $\mathrm{Pr} = 6.7$. A route to those LSCs from regular roll structures observed at slightly supercritical conditions, however, has not been clarified yet.

The so-called "Busse balloon" describes the stable region in the Ra – wave number plane where two-dimensional (2D) steady roll structures occur after the onset of convection. This domain of stability is bounded by several kinds of instabilities the exact course of the boundary lines being determined by the Pr number. (e.g., Ref. 10). Exceeding these limits by increasing the Ra number, the pattern of convection rolls easily becomes time dependent due to the oscillatory instability at slightly supercritical Ra, and traveling waves propagate in the direction of the roll axis [11–13]. The effect of traveling waves on the roll structure beyond the boundary of the Busse balloon was studied by numerical simulations [14, 15]. Krishnamurti [1] investigated the transition from steady to time dependent flow at a slightly supercritical Ra number by temperature fluctuations in a fluid layer of mercury. Further increase of Ra leads to the transition to turbulence, while in the case of small Pr numbers the transition occurs at lower Ra numbers [1, 2]. Laboratory experiments [1, 16] came to the conclusion that the Busse balloon shrinks to a very narrow domain for very low Pr numbers, $\mathrm{Pr} \sim O(10^{-2})$.

Nevertheless, Nevertheless, the evolution of the LSC structure in low Pr convection on the way to thermal turbulence is not fully understood yet. This situation provides the motivation for the experimental study on convection in a liquid metal layer presented here. Liquid metals as representatives of very low Pr fluids are opaque, so usual optical methods for flow visualizations are not applicable for these fluids. Most of the previous experimental studies on liquid metal convection have therefore limited themselves to the heat transfer in the system and the measurements of temperatures and their fluctuations [17–22]; Temperature fluctuation measurements suggest flow transition on oscillatory rolls. However, direct measurements of flow velocities have not been realized, which is why spatio-temporal characteristics of low Pr convection are still largely unclear. Simultaneous measurement of velocity profiles and temperature fluctuations could provide a better understanding of the development and properties of large-scale circulations in low Pr thermal turbulence.

The ultrasonic velocity profiling (UVP) [23, 24] is the most straightforward tool to measure and visualize flow fields of opaque fluids such as liquid metals. It has already been applied for investigations of low-Pr thermal turbulence. First measurements of instantaneous velocity distributions in liquid metal RBC were reported by Mashiko *et al.* [25] for a cylinder ($\Gamma = 1$) filled with mercury. Tsuji *et al.* [26] detected various complex modes of large-scale circulations undergoing periodic oscillations in cylindrical geometries of aspect ratios around unity ($\Gamma = 0.5$, 1 and 2) in the range of large Pr numbers ($10^6 < \mathrm{Pr} < 10^{10}$). Yanagisawa *et al.* [27] studied flow patterns occurring in liquid gallium in a rectangular vessel ($200 \times 50 \times 40$ mm) and showed the existence of oscillatory roll structures up to $\mathrm{Ra} \sim 10^5$. In this configuration, the direction of rolls was strictly constrained by the geometry of the vessel resulting in an orientation of the roll axes parallel to the shorter horizontal length of the container.

The main objective of this study is to identify and characterize coherent flow structures in low Pr turbulent convection inside a square box ($\Gamma = 5$) at moderate Ra numbers, $O(10^4)$ – $O(10^5)$. The focus is particularly on the transition from roll-like flow regimes, their structures are closely related to the commonly known onset rolls, to a cell-like, whose features resembles essential properties of a LSC. The occurrence of developed thermal turbulence is expected for the highest Ra numbers considered within this study. Multiple orthogonally superimposed horizontal velocity profiles are measured in the fluid layer at different heights by UVP. The measured data allow for identifying the large-scale three-dimensional (3D) flow structures. Thermocouples are used to monitor the corresponding temperature fluctuations simultaneously. Following the details of experimental setup and procedure explained in Sec. II, the development of spatio-temporal characteristics of the LSC with increasing Ra is investigated in Sec. III A, Sec. III B and Sec. III C. The statistical turbulent properties of the convection are evaluated on the basis of the measured temperature fluctuations in Sec. III D. In Sec. IV A a scaling law describing the variation of the size of typical flow structures will be suggested and compared to the results obtained in air layers using different geometries [5, 28]. Variations of horizontal scale of the coherent structures are further discussed in Sec. IV B.

II. EXPERIMENTAL SETUP

Schematic sketches of the experimental setup, the square vessel filled with the fluid and arrangements of the ultrasonic measurement lines, are shown in Fig. 1, (a) top and (b) side view. The vessel is identical to that used in our previous studies [29, 30] to which the reader is referred here for a detailed description of the setup. The lateral walls of the vessel are made of 10-mm-thick PVC to attain thermal insulation. The fluid layer has a square horizontal cross section of 200 mm × 200 mm and a height of 40 mm, giving an aspect ratio of five. It is sandwiched between the top and bottom copper plates which

ensure isothermal heating and cooling. The temperatures of each copper plate, T_h and T_c, are controlled by water flowing through channels inside the plates. The temperature values are monitored during the experiments by thermocouples embedded in the copper plates. The vertical temperature difference is determined as $\Delta T = T_h - T_c$. The available range from 0.36 ° C to 15.93°C is restricted by the requirement to ensure isothermal conditions on the surfaces of the copper plates. The test fluid is the eutectic alloy $Ga^{67}In^{20.5}Sn^{12.5}$ whose kinematic viscosity is $\nu = 3.4 \times 10^{-7}$ m^2/s and thermal diffusivity is $\kappa = 1.05 \times 10^{-5}$ m^2/s, giving Pr = 0.03 (the thermo-physical properties are summarized in Plevachuk *et al.* [31]). Considering a value of the density of $\rho = 6360$ kg/m^3 and a thermal expansion coefficient of $\alpha = 1.24 \times 10^{-5}$ K^{-1}, the Ra number can be varied in the range from 7.9×10^3 to 3.5×10^5.

The UVP technique [23, 24] and thermocouples were used for obtaining instantaneous velocity profiles and point-wise temperature fluctuations of thermal turbulence. Ten ultrasonic transducers with a basic frequency of 8 MHz were mounted horizontally inside holes drilled into the two side-walls of the vessel and contacted directly with the test fluid. The gray lines shown in Fig. 1 indicate the orthogonal measuring lines. Four transducers labelled from CH1 to CH4 in the figure were installed at a distance of 10 mm to the top plate ($z = 30$ mm) and the other six transducers labelled from CH5 to CH10 were set at a distance of 10 mm to the bottom plate ($z = 10$ mm). The ultrasound Doppler approach provides instantaneous profiles of the velocity component projected onto each measurement line, $u(x,t)$ and $v(y,t)$, respectively. The horizontal velocity components, (u, v), are obtained at the intersection points of the measurement lines represented as white circles in Fig. 1(a). Temporal, spatial and velocity resolutions of the UVP measurements are 1.2 s, 1.4 mm and 0.5 mm/s, respectively. The velocity profiles along each measurement line were acquired sequentially by multiplexing. A thermocouple was positioned in the fluid layer at $x = 100$ mm and $y = 120$ mm, and 3 mm below the top plate ($z = 37$ mm) (see T in Fig. 1) to measure temperature fluctuations with a sampling rate of 10 Hz.

III. MEASUREMENT RESULTS

A. Transition of coherent structures

Systematic flow measurements were conducted in the Ra number range from 7.9×10^3 to 3.5×10^5. The analysis of the measured flow profiles discloses the existence of four different flow structures in this range. The investigation of the transitions between these coherent structures for varying Ra numbers is a key point of this study. In the square fluid vessel an oscillatory roll-like flow is observed as coherent structure for Ra numbers around 10^4 which was not necessarily expected before.

Such a roll-like structure occurring at lower Ra numbers (Ra $= 1.1 \times 10^4$) is shown by spatio-temporal velocity maps in Fig. 2 (a)–(d), where the velocity data were measured parallel to the x-axis [(a) CH1 and (c) CH6, see Fig. 1] and to the y-axis [(b) CH4 and (d) CH9], respectively. The lines of CH6 and CH9 crosses at the center of the vessel at a height of $z = 10$ mm while the sensors CH1 and CH4 record the velocity a height of $z = 30$ mm. The velocity maps (a) and (c) show wavy patterns of four stripes corresponding to four rolls whose time-averaged orientations are aligned parallel to the y-axis. Since the profiles CH1 and CH6 were measured at different heights, they capture the top and bottom sides of the convection rolls. Thus, the direction of the flow velocities in the plot appears opposite. Such a roll pattern is typically observed on all other measurement lines aligned parallel to the x-axis. The period of the oscillation is about 100 s which is the same order of magnitude as the thermal diffusion time of the fluid layer, $L^2/\kappa \approx 153$ s. Its relation to the turn over time of the convection roll is discussed in Sec. IV B. The velocity maps (b) and (d) show the flow pattern which was measured on the measuring lines parallel to the y-axis. It is dominated by spots, those are smaller than 10 mm and synchronized with the wavy motion observed in (a) and (c). The plots suggest that these wavelike structures propagate from the wall into the interior of the convection cell. The maximum velocity measured for the flow profiles along the y-direction is approximately half the value of that in the x-direction. This "four-roll structure" is stable and keeps the direction of initial roll axes throughout the measurement time over 5000 s, once the structure emerges.

With a small increase in the Ra number to 2.1×10^4, the roll-like structure loses its regularity with respect to the rotation axis as shown in the spatio-temporal velocity maps in Fig. 2(e)–(h). In this flow state, wave-like patterns are observed, which can be interpreted as four or three convection rolls whose axes are aligned alternately parallel to the x or the y axis. It is noticeable that the basic structure of the flow is not maintained over the entire measuring time. In a first period from 0 s to about 350 s, the velocity map recorded near the side wall by transducer CH4 [Fig. 2(h)] shows a transformation between different structures, but at the centerline, transducer CH9 shown in Fig. 2(h), a three-roll structure aligned parallel to the x axis survives ["three-roll (x)" in Fig. 2; here (x) means roll axis is in the direction of x]. The velocity map in Fig. 2(f) shows that additional rolls emerge near the wall and then disappear after some time. The flow measurements along the x-axis ["three-roll (x)" in Fig. 2(e) and (g)] do not show a dominant roll structure at that time. The velocity field along the x-direction looks more complicated, propagating wave-like structures are observed in the center of the fluid layer. In the time window between 350 s and 750 s, three-roll structures become visible in the measurements along the x-direction which means that the orientation of the convection rolls must have rotated by 90° ["three-

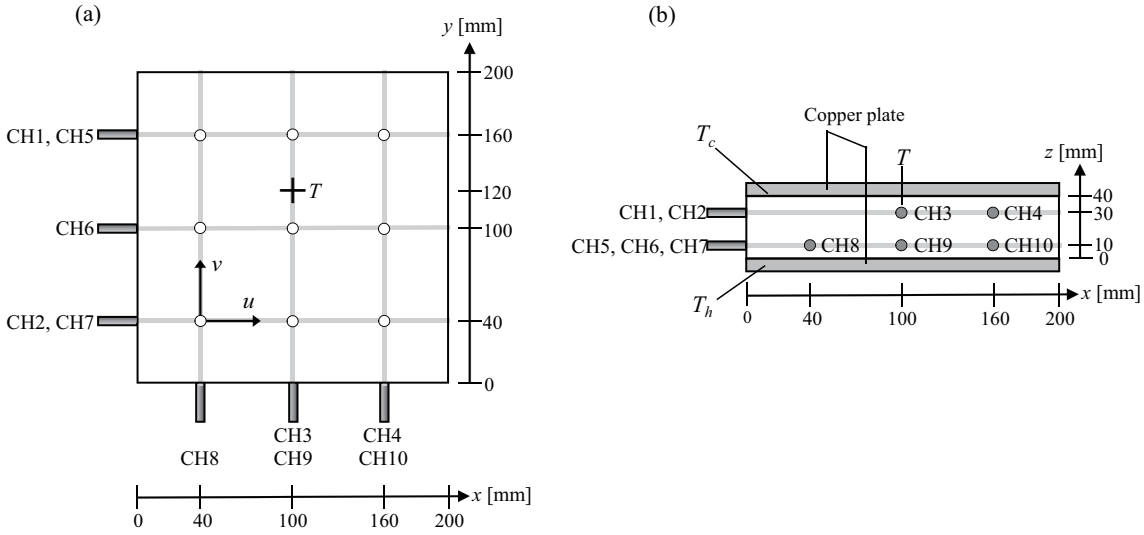

FIG. 1. Experimental setup and arrangement of measurement lines: (a) top view and (b) side view, where gray lines indicate the measurement lines of UVP

roll (y)" in Fig. 2]. This clearly shows a competition between rolls in x- or y- direction. After around 750 s, the flow structure shows a spontaneous transition to a wavy four-roll structure ["four-roll (y)" in Fig. 2]. All this together demonstrates, that there is no stable flow in this parameter range. Over a longer period of time, neither 3- or 4-roll regimes remain stable, nor is the orientation of the rolls along the x or y direction constant. More complicated patterns, like rolls with an axis that runs diagonally through the convection cell, could be formed. The transitions between the different structures occur in intervals of some hundred seconds. This state may be understood as an intermediate regime of "four-roll structure" to "three-roll structure", therefore, this flow state may be referred to as a "4-3 roll transition state".

In turn, roll-like structures with constant number of rolls are observed again by further increase in Ra as shown in Fig. 2(i)–(l) for $\mathrm{Ra} = 4.6 \times 10^4$. The velocity maps (i) and (k) present a fluctuating pattern with three dominating stripes corresponding to three rolls whose axes are oriented in y-direction. Compared to the regimes observed at smaller Ra numbers, the magnitude of velocity is significantly larger and the period of the flow oscillations appears to be shorter. The maximum velocity in (l) is about 70% of the value found in (k). This suggests that the dominant structure is still a three-roll structure with axes in the y-direction, although the difference in velocity along the orthogonal measurement lines is not as great as determined in the case of smaller Ra numbers. The latter finding is a clear indication of the growing three-dimensional nature of the flow. This "three-roll regime" is quasi-stable and keeps the direction of roll axes for some thousand seconds, but in other measurements conducted at the same Ra number one could also observe sudden changes in the direction of the rolls with corresponding flow reversals.

The roll-like structures completely disappear at $\mathrm{Ra} = 1.8 \times 10^5$ as shown in Fig. 2(m)–(p). Velocity maps obtained on the center lines crossing at the central point of the vessel, presented in Fig. 2(o) and (p), show a wavy band dividing the vessel into two parts. Flow structures are heading for the center of the vessel from each side wall, hence, an upwelling flow at the center is expected. Compared to the previously discussed measurements at low Ra numbers, the absolute values of the velocity have continued to increase. The period of the oscillation is shorter than that in the former regime; it is almost half of the thermal diffusion time of the fluid layer. The flow maps in Fig. 2(m) and (n) which were recorded along measuring lines located closer to the side walls show a more fragmented pattern. The magnitudes of velocities depend on the measuring position; the maximum velocities near the wall are about half of the values obtained on the center lines. There is no significant difference in the behavior of the flow with respect to their alignment in the x- and y-directions. The main structure is, therefore, a 3D oscillatory flow structure dividing the vessel into two parts as observed on the center lines. We named this flow state as "cell structure". There is an overlapped range of Ra between "three-rolls structure" and "cell structure". Sudden changes of the flow structures from the three-roll structure to the cell structure were observed around $\mathrm{Ra} = 6.0 \times 10^4$.

B. Details of the coherent structures

In the present experiment, simultaneous measurements were performed using 6 ultrasonic transducers in a horizontal plane at $z = 10$ mm (from CH5 to CH10 in

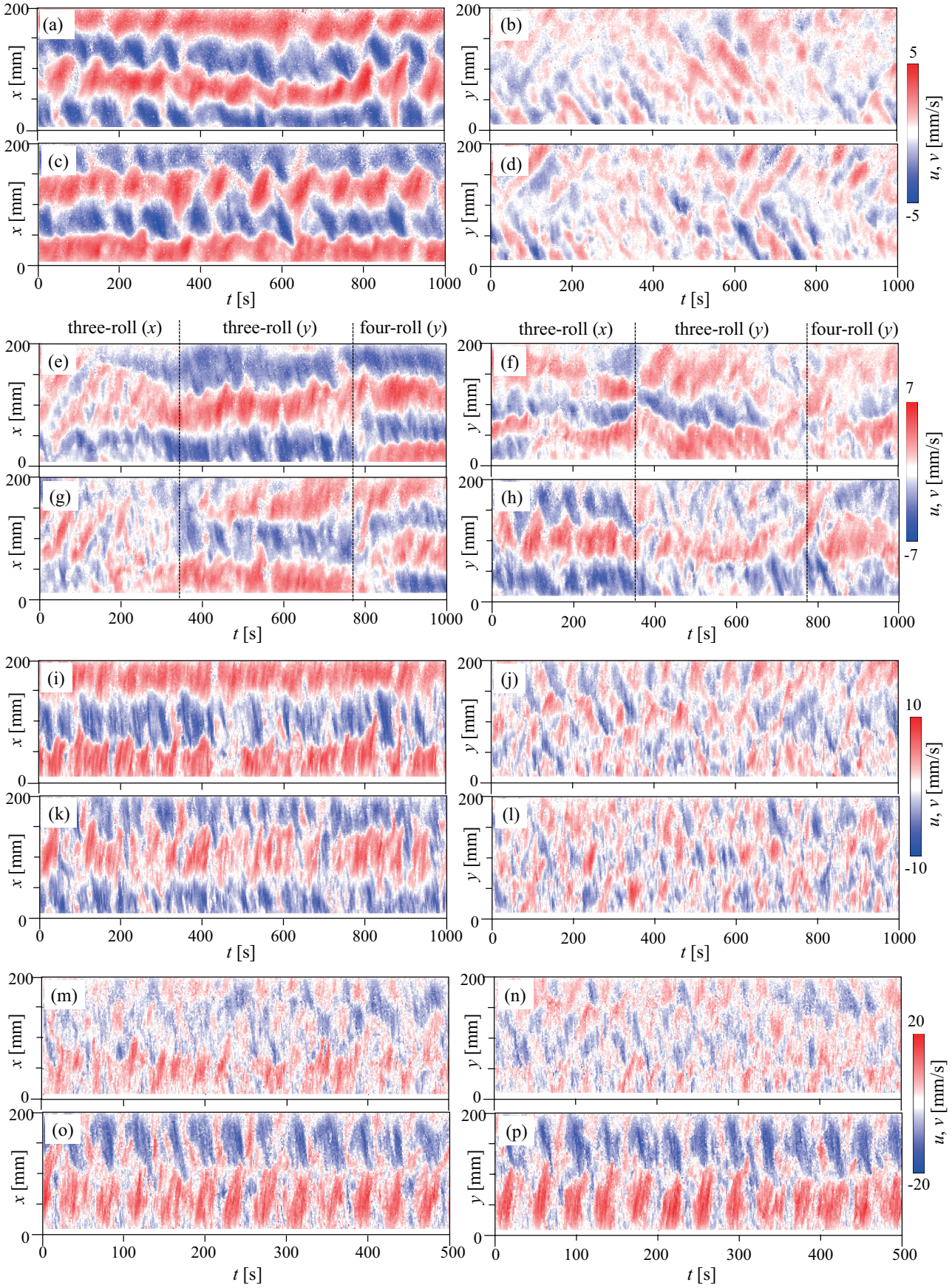

FIG. 2. Spatio-temporal velocity distributions for four cases of Ra along the measurement lines of transducers CH1, 4, 6, and 9 in this order in each set: (a)–(d) $\mathrm{Ra} = 1.1 \times 10^4$ (four-roll structure), (e)–(h) $\mathrm{Ra} = 2.1 \times 10^4$ (four-three roll transition), (i)–(l) $\mathrm{Ra} = 4.6 \times 10^4$ (three-roll structure), and (m)–(p) $\mathrm{Ra} = 1.8 \times 10^5$ (cell structure)

Fig. 1). Since the measurement lines cross perpendicularly to each other in the fluid layer, the 2D velocity information (u, v) can be obtained at nine intersection points. Scatter diagrams of (u, v) were compiled at those intersection points and time-averaged velocity vectors were calculated on the horizontal plane, $\boldsymbol{V}_H(\overline{u}, \overline{v})$, to deduce details of the 3D coherent structure for each flow regime. In Fig. 3(a), a scatter diagram for the "four-roll structure" at $\mathrm{Ra} = 1.1 \times 10^4$ is shown [compare Fig. 2(a)–(d)]. The number of samplings for each diagram is 320. At the all intersection points, the values of the y-component of the velocity v are nearly equally distributed around $v = 0$. Corresponding distributions of the x-component u differ significantly depending on the respective measurement line. A clear tendency for an inward flow becomes obvious on the lines at $y = 40$ mm and $y = 160$ mm, while an almost equal distribution around zero can be observed at $y = 100$ mm. In addition, the distributions of u show a larger variance than v at the all points. Fig. 3(b) presents a schematic view of the flow regime and the time-averaged velocity vectors, $\boldsymbol{V}_H(\overline{u}, \overline{v})$. Assuming an ideal four-roll regime, the center line at $x = 100$ mm runs exactly between two adjacent convection rolls, while the other two lines are located inside the outer rolls with opposite rotation. This is in accordance with the velocity vectors in Fig. 3. Obviously, the relative position of the measurement lines with respect to the convection rolls changes for the three-roll structure (see Fig. 4). These are now closer to the center of the convection rolls. Thus, the vectors in Fig. 4(b) very clearly reflect the directions of rotation of the three rolls. Moreover, it is worth to note that the scattering ranges of both u and v in Fig. 4(a) become wider in comparison with the four-roll structure (Fig. 3(a)), and $\boldsymbol{V}_H(\overline{u}, \overline{v})$ reaches larger values [Fig. 4(b)].

The scatter diagrams of (u, v) displayed in Fig. 5(a) correspond to the velocity maps in Fig. 2(m)–(p) which represent a new type of flow structure at $\mathrm{Ra} = 1.8 \times 10^5$ which can no longer be interpreted as a roll structure and was called a cell-like regime. The vectors in Fig. 5(b) give a characteristic pattern. Obviously, the fluid above the heater plate flows inward toward the center of the convection cell where it rises upwards indicated by the time-averaged zero values of both velocity components at the central position. The circulation loop is closed by a diverging flow beneath the cooling plate and a descending motion towards the bottom near the midpoints of all side walls. Smaller convection cells with opposite flow direction exist apparently in the corners of the fluid container. The flow vectors are directed towards the corners and the velocity magnitudes are smaller than those at the outer intersection points on the center lines. These results allow reconstructing a cell-like structure in the vessel, which has upwelling flows at the center and right in the four corners as the schematic view shows in Fig. 5(c). Either cell structures with upwelling or downwelling at the center are observed for sufficiently large Ra numbers ($\mathrm{Ra} \geq 6.8 \times 10^4$). The selection of the flow direction might be determined by non-ideal thermal conditions at the sidewall boundaries. Once one of the two cell structures is formed, it is stable and sustained for a very long time over a few thousand seconds.

The ratio of the time-averaged root mean square (rms) velocities, U_x/U_y recorded along the two measurement lines crossing at the center of the vessel at $z = 10$ mm (CH6 and CH9) are presented as a function of the Ra number in Fig. 6, where

$$U_x = \overline{\sqrt{\frac{1}{5L}\int_0^{5L} u^2(x,t)dx}},\ U_y = \overline{\sqrt{\frac{1}{5L}\int_0^{5L} v^2(y,t)dy}};$$

cross-bars in the equation indicate time-averaged values. The occurrence of the diverse coherent flow structures is marked by different symbols in the diagram. This ratio represents the balance of horizontal velocity in either direction x or y; it is expected to approach zero for perfectly 2D roll structures, while it should become close to unity for fully 3D coherent structures. The small values found at lower Ra numbers for the "four-roll structure" and the "three-roll structure" indicate a distinct tendency to two-dimensionality although the convection rolls are subject to significant 3D disturbances which are most pronounced in the case of the 3-roll regime [see also Fig. 2(i)–(l) and Fig. 4] The calculation of the velocity ratio for the "four-three transition" regime was conducted in a time interval, at which the roll structures appear to be stable excluding flow pattern transitions. The velocity ratio reaches unity when the transition to the cell structure occurs.

C. Temporal characteristics of coherent structures

In the range of Ra numbers examined in this study, quasi-periodic oscillations of the coherent structures are observed in the spatio-temporal velocity maps as mentioned in Sec. III A. The typical frequencies of oscillations in the flow patterns, both rolls and cells, are obtained from the spatially averaged power spectral densities (PSDs) of the velocity maps as described below. Smoothing of the spectra obtained by Fourier transform is achieved by dividing the velocity time series into multiple time intervals of around 200 s. The spectra are calculated for each time interval and for each measurement point along the measurement lines CH1, CH4 (x-direction), CH6 and CH9 (y-direction, see also Fig. 2). Then, these interim results are averaged both in space and in time. The PSDs for the four-roll regime at $\mathrm{Ra} = 1.1 \times 10^4$ are shown in Fig. 7(a). The PSDs have dominant peaks around $f = 0.010$ Hz corresponding to the oscillation frequency, f_{OS}, of the wavy flow patterns shown in the velocity maps of Fig. 2(a–d). The PSDs at $\mathrm{Ra} = 2.1 \times 10^4$ are shown in Fig. 7(b) for the same measurement lines. Here, averaging over domains with different roll structures leads to a disappearance of the dominant peaks; The transition between different flow structures in this regime is accompanied by a change

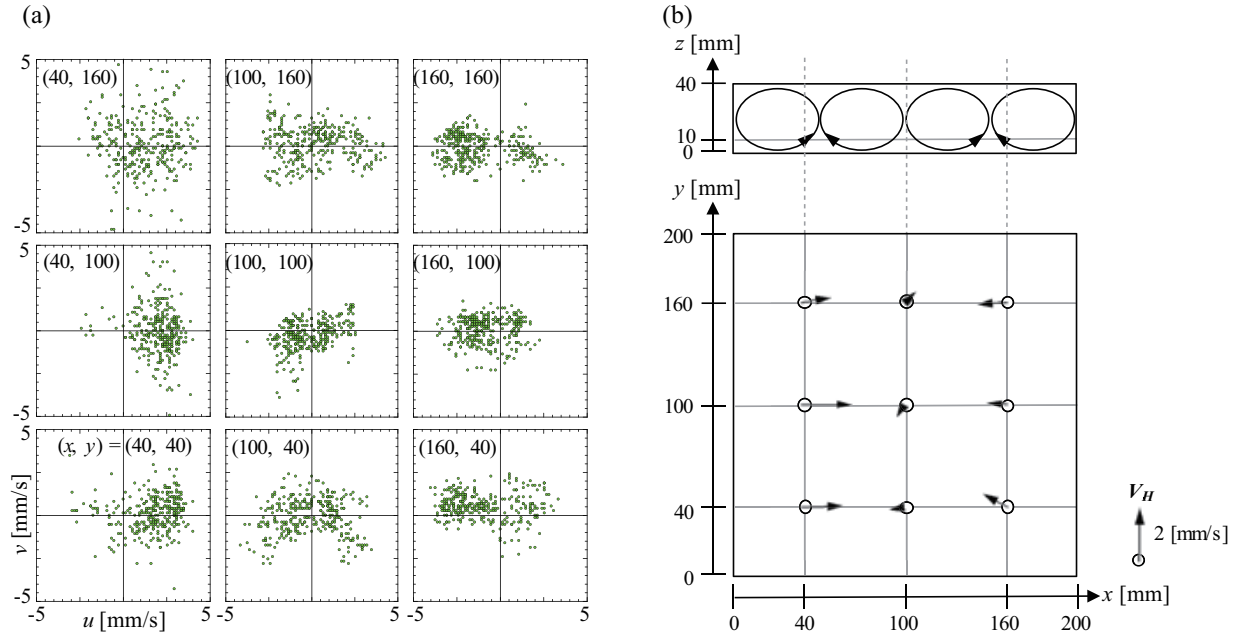

FIG. 3. (a) Scatter diagram of (u, v) at nine intersection points on $z = 10$ mm, and (b) time-averaged 2D velocity vectors on the horizontal plane, $\boldsymbol{V}_H$ $(\overline{u}, \overline{v})$ with a schematic image representing a side view of the roll-like structure expected from the results; Ra $= 1.1 \times 10^4$ and "four-roll structure" regime

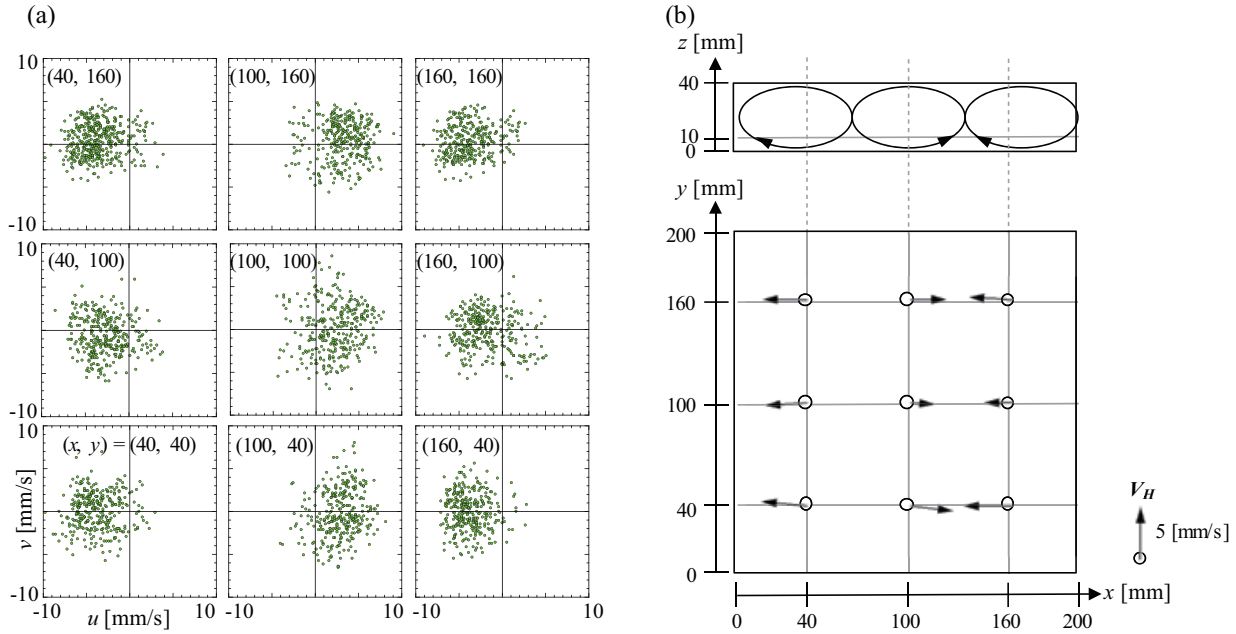

FIG. 4. (a) Scatter diagram of (u, v) at nine intersection points on $z = 10$ mm, and (b) time-averaged 2D velocity vectors on the horizontal plane, $\boldsymbol{V}_H$ $(\overline{u}, \overline{v})$ with a schematic image representing a side view of the roll-like structure expected from the results; Ra $= 4.6 \times 10^4$ and "three-roll structure" regime

in the characteristic oscillation frequencies. The PSDs calculated for the three-roll regime at Ra $= 4.6 \times 10^4$ [Fig. 7(c)] show a broad peak in the frequency range from $f = 0.01$ Hz to $f = 0.02$ Hz. Here, the typical frequency of $f_{\mathrm{OS}} = 0.016$ Hz results from averaging of the PSDs within this frequency range. PSDs for the cell structure regime at Ra $= 1.8 \times 10^5$ are shown in Fig 7(d). All spectra show sharp peaks at 0.025 Hz corresponding to the

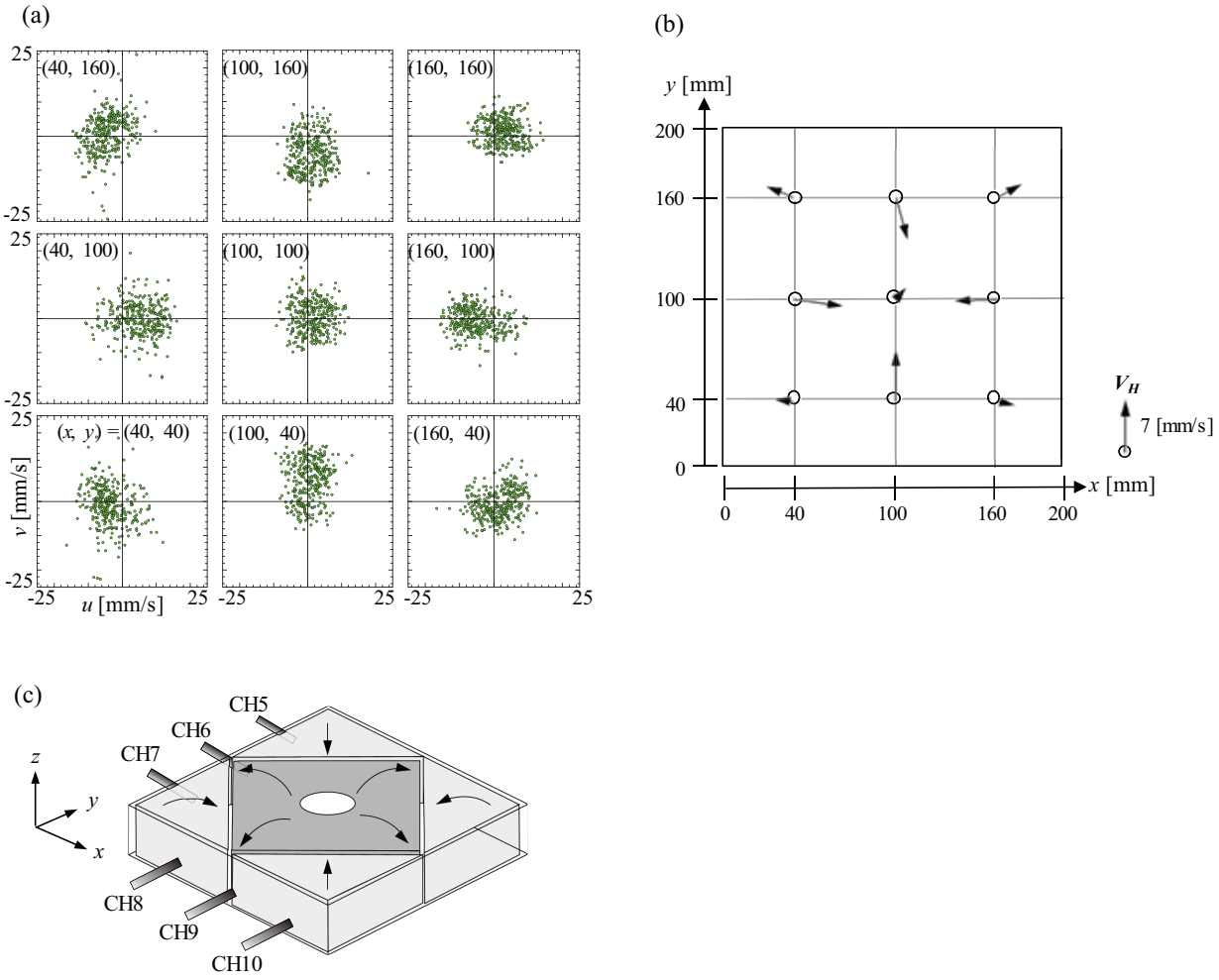

FIG. 5. (a) Scatter diagram of (u, v) at nine intersection points on $z = 10$ mm, (b) time-averaged 2D velocity vectors on the horizontal plane, $\boldsymbol{V}_H$ $(\overline{u}, \overline{v})$, and (c) a schematic image of 3D structure expected from the results; Ra $= 1.8 \times 10^5$ and "cell structure" regime

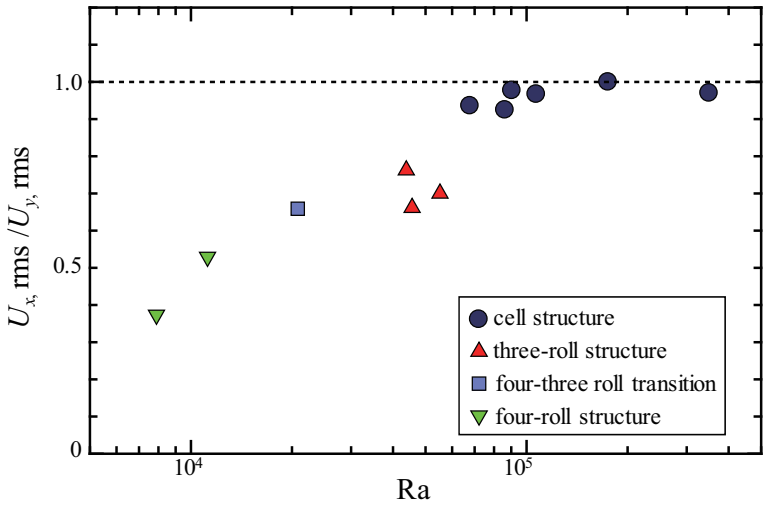

FIG. 6. Ratios of spatial rms velocities measured by CH6 and CH9 at different Ra numbers

oscillations observed in the velocity maps. In summary, it can be stated that the typical frequencies of the oscillation increase with increasing Ra, which will be discussed in further detail in Sec. IV A.

To investigate the 3D oscillations of the cell structure in detail, time variations of u at $(x, y) = (50, 100)$ mm and v at $(100, 50)$ mm are plotted in Fig. 8(a). The fluctuations show quasi-regular oscillations corresponding to the typical frequency, $f_{\mathrm{OS}} = 0.025$ Hz. Obviously, the signals of the two velocity components are in anti-phase. Spatial profiles of the phase at the frequency component corresponding to $f_{\mathrm{OS}} = 0.025$ Hz are calculated by Fourier transformation [Fig. 8(b)]. This diagram reveals a phase jump in the middle of the fluid vessel. One possible interpretation of these results suggests that a reciprocal elliptical deformation of the central cell as shown in Fig. 8(c) could be the reason for the oscillations observed in the measured velocity data.

D. Statistical characteristics of temperature fluctuations

This section focusses on the statistical characteristics of thermal turbulence. Temperature fluctuations measured directly in the fluid layer are shown in Fig. 9(a)–(d). These temperature time series result from a moving average over a window of 5 s and a normalization with the temperature difference ΔT. The fluctuations obtained at $\mathrm{Ra} = 1.1 \times 10^4$ [Fig. 9(a)] does not show clear periodic oscillations as observed in the spatio-temporal velocity maps in Fig. 2(a) and (c). This is due to the fact that the temperature difference applied between the top and the bottom plate is very small for the smallest Ra number. Hence, the magnitude of the temperature fluctuations is only slightly above the noise level of the measurement. The temperature fluctuations grow with an increase in the Ra number to 2.1×10^4 [Fig. 9(b)]. However, no clear periodicity becomes visible which is likely due to the distinct intermediate character of this flow regime. Pronounced quasi-periodic oscillations appear in the temperature signal at higher Ra numbers [$\mathrm{Ra} = 4.6 \times 10^4$ in Fig. 9(c) and $\mathrm{Ra} = 1.8 \times 10^5$ in Fig. 9(d)].

The corresponding PSDs of the temperature fluctuations are presented in Fig. 9(e). The same procedure was applied for smoothing the spectra as already described for the velocity. The thermal energy spectrum model for low-Pr turbulence predicts a $-5/3$ slope for the inertial-convective subrange, and a $-17/3$ slope for the inertial-conductive subrange [32]. The corresponding slopes are indicated in the figure as dashed lines. The shape of the PSDs changes depending on Ra, and seemingly, the spectra approximate the predicted slopes with increasing Ra number. This leads to the statement that the convective motion is approaching the state of fully developed thermal turbulence for Ra numbers of 1.8×10^5 and beyond. Herewith, it is confirmed that 5he cell structure, which has been recognized as the large scale circulation at this Ra number, occurs under the condition of thermal turbulence (e.g. Ref. 3 and 4).

IV. DISCUSSION

A. Scaling of the size of coherent structures

In this experiment, the wavelength of coherent flow structure increases systematically, but discretely with the increase of Ra due to the restriction by the finite horizontal dimension of the vessel. The purpose of this section is to examine whether one can derive a law for continuous variation of the size of coherent structures from the experimental data available in terms of flow velocity and oscillation period, despite the geometric constraint of the container.

Lam *et al.* [33] proposed three different velocity scales as the representative velocity of the flow structure that can be estimated from limited information obtained by experiments: (i) the maximum velocity on time-averaged velocity profiles, (ii) the root mean square (rms) values of the velocity fluctuations, and (iii) the velocity calculated from the typical oscillation timescale of the structures. We select the rms velocity as the most robust value to be derived from experimental data for estimating the turn-over time. The Rayleigh number dependence of the representative flow velocity U_{rms} is shown in Fig. 10(a), where the rms velocity U_{rms} is calculated from spatio-temporal velocity maps as space-time rms values; the spatio-temporal velocity maps underlying the calculations are recorded along either CH6 or CH9, depending on which of both was aligned perpendicular to the rotation axis of rolls in the roll regimes. U_{rms} is converted into a non-dimensional form using the thermal diffusivity κ of the fluid and the layer thickness L. Different symbols in the figure indicate different regimes categorized in Sec. III A. The velocity variation can be fitted by a unified power law,

$$U_{\mathrm{rms}} L/\kappa = 0.059 \mathrm{Ra}^{0.50 \pm 0.02}, \tag{1}$$

where the exponent is obtained from the least square approximation of the measurement results. Similar values of the exponent around 0.5 (0.46...0.52) were also obtained by other experimental [17, 27, 34] and numerical studies [35] for low Pr fluid turbulence. From this point of view, this scaling seems quite robust, not least because the other experiments used different combinations of aspect ratios and liquid metals, in particular mercury ($\mathrm{Pr} = 0.024$) and $\Gamma = 1$ [17], gallium (0.025) and $\Gamma = 1.25$ [27], or gallium and $\Gamma = 5$ [34]. In the last two studies the maximum velocity measured within the convection rolls was used as the representative velocity in the both cases. The typical oscillation frequency f_{OS} also changes with the Rayleigh number as shown in Fig. 10(b), where the frequency is defined as reported in Sec. III C. The values are normalized with the thermal

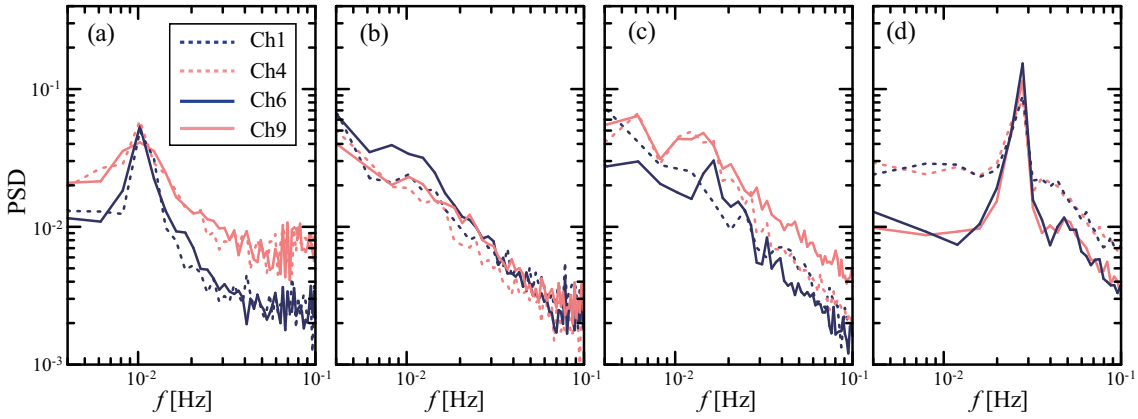

FIG. 7. Spatially averaged PSDs calculated from spatio-temporal velocity maps measured by CH1, 4, 6, and 9 (see Fig. 1) at (a) $\mathrm{Ra} = 1.1 \times 10^4$ (four-roll structure), (b) $\mathrm{Ra} = 2.1 \times 10^4$ (four-three rolls transition), (c) $\mathrm{Ra} = 4.6 \times 10^4$ (three-roll structure), and (d) $\mathrm{Ra} = 1.8 \times 10^5$ (cell structure)

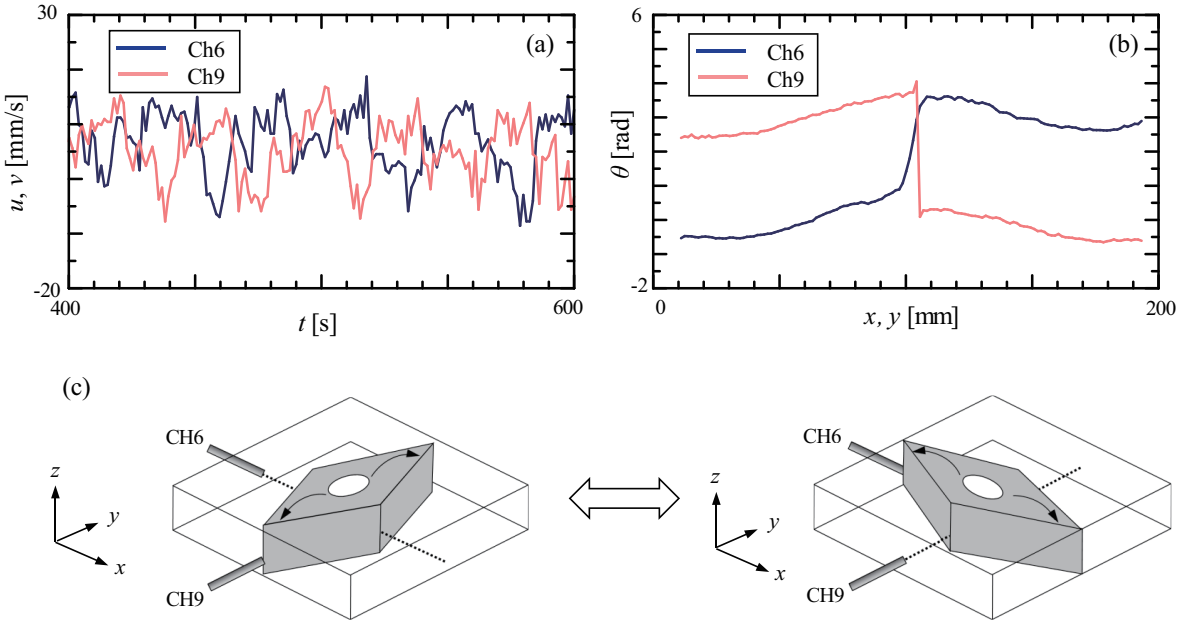

FIG. 8. (a) Time variations of u at $(x, y) = (50, 100)$ mm measured by CH 6 and v at $(100, 50)$ mm measured by CH9 at $\mathrm{Ra} = 1.8 \times 10^5$, (b) corresponding phase profiles at the oscillation frequency, $f_{\mathrm{OS}} = 0.025$ Hz, and (c) a schematic plane image of oscillations of the cell structure

diffusion time scale. Applying the least square method gives a power law approximated as

$$f_{\mathrm{OS}} L^2/\kappa = 0.039 \mathrm{Ra}^{0.38 \pm 0.02}. \tag{2}$$

The exponent of 0.38 is smaller than that of the typical flow velocity 0.5 in Eq. (1), namely the oscillation frequency increases with Ra more gradually than the velocity. By using the oscillation frequency f_{OS}, we define the oscillation period τ_{OS} as $1/f_{\mathrm{OS}}$.

Previous studies suggested that the period of wavy motions on convection rolls observed near the onset of convection for $\mathrm{Pr} \sim 1$ corresponds to the turn-over time, the time scale of one circulation of a fluid element within a convection roll (e.g., Ref. [13]). The turn-over time τ_{TO} is estimated in this system using the variable horizontal wavelength of the flow structure λ_{H}, the fluid layer thickness L, and the representative flow velocity U_{rms} as

$$\tau_{\mathrm{OS}} = \frac{\pi \left(\lambda_{\mathrm{H}}/4 + L/2 \right)}{U_{\mathrm{rms}}}, \tag{3}$$

where $\pi(\lambda_{\mathrm{H}}/4 + L/2)$ represents an estimation for the path-length of a circulation assuming elliptic path-lines with half of the wavelength $\lambda_{\mathrm{H}}/2$ as the major and the layer height L as the minor axis length. Here, the wavelength is determined from the spatial periodicity of the flow structures and turns out to be $2.5L$ (four-rolls struc-

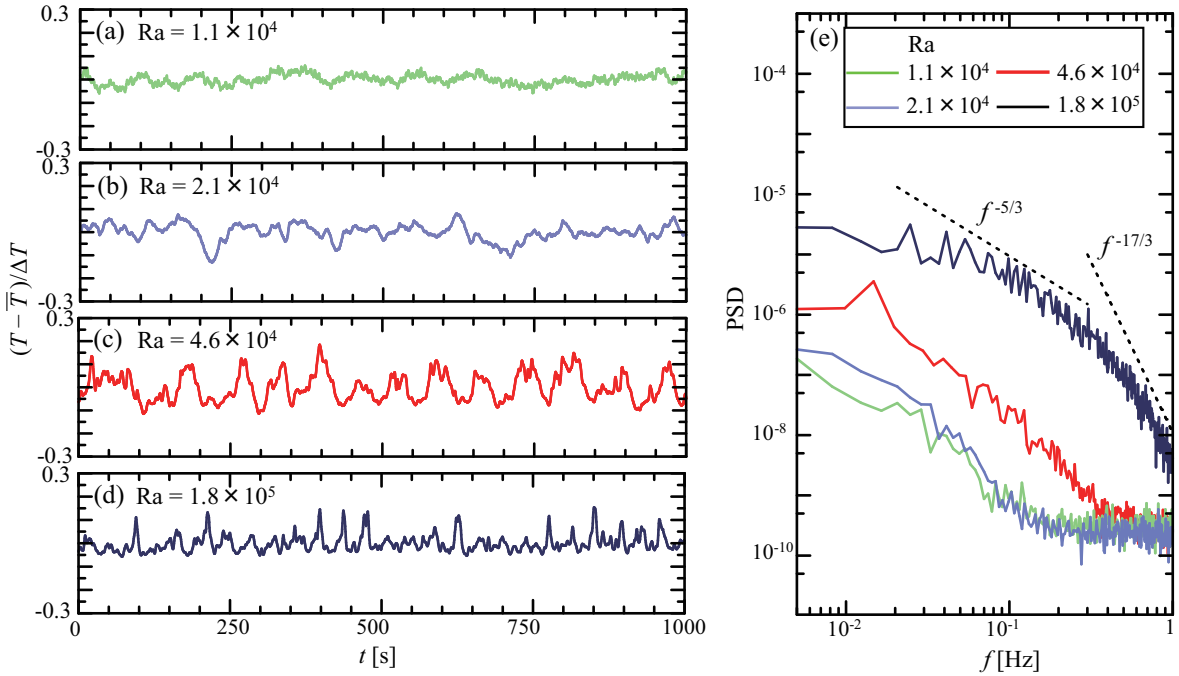

FIG. 9. Temperature fluctuations measured in the fluid layer (see Fig. 1 for the measurement point "T") at (a) Ra $= 1.1 \times 10^4$ (four-roll structure), (b) Ra $= 2.1 \times 10^4$ (four-three transition), (c) Ra $= 4.6 \times 10^4$ (three-roll structure), (d) Ra $= 1.8 \times 10^5$ (cell structure), and (e) PSDs of the temperature fluctuations. The dashed lines indicate the slopes of $-5/3$ and $-17/3$.

ture), $3.3L$ (three-rolls structure) and $5L$ (cell structure) considering the aspect ratio $\Gamma = W/L = 5$. To clarify the relation between oscillation period and turn-over time, the ratio τ_{OS} to τ_{TO} is plotted against Ra in Fig. 10(c); It indicates

$$\tau_{\mathrm{OS}} \approx c\tau_{\mathrm{TO}}, \tag{4}$$

where c is constant ~ 1. Thus, a striking feature of the relationship is that it reaches a value of about one throughout the entire Ra number range of the present study. Obviously, Eq. (4) is a common feature for the convection in all regimes represented by Eq. (3). For deriving a scaling relation for λ_{H} as a function of the Ra number, Eq. (1) and Eq. (2) are inserted into Eq. (3). The subsequent conversion to λ_{H} yields

$$\lambda_{\mathrm{H}} \approx 1.93/c\ \mathrm{Ra}^{0.12} - 2. \tag{5}$$

The power law in Eq. (5) describes a continuous variation of λ_{H} with Ra, while the original variation of λ_{H} obtained in the present experiment is discrete due to geometrical restrictions in the vessel of aspect ratio 5. The resulting curve of the power law (taking a value of $c = 1.2$ into account) is plotted in Fig. 11 together with experimental and numerical data from the literature for Pr ~ 0.7 [5, 28] and the discrete values for λ_{H} found in the present study. A detailed discussion of this figure can be found in the next section.

B. Transitions between the coherent structures

Four different flow structures were identified in the parameter range considered in this study. The regime diagram by Krishnamurti [1] does not suggest the existence of an oscillatory roll-like regime at Ra $\sim 10^4$ as found in our experiments. Basically similar flow patterns consisting of convection rolls, which are subject to distinct 3D disturbances, were also observed in experiments with imposed horizontal magnetic fields carried out at similar Ra numbers in the same convection cell [30]. The statistical analysis of the temperature fluctuation reveals, however, a significantly higher level of turbulence in the present case [see Fig. —9(e)], while the influence of the magnetic field obviously has a stabilizing effect on the roll structure [30]. Regardless of the high turbulence level, the roll-like structures exist up to a Ra number of about 6.8×10^4 before a transition to a cell structure occurs.

Hebert *et al.* [37] investigated the onset of Rayleigh-Bénard convection in cylindrical containers. For aspect ratios $1.58 \leq \Gamma \leq 3.26$ just above $\mathrm{Ra_c}$, they reported the formation of a concentric roll corresponding to an azimuthal Fourier mode with the wave number $m = 0$. As already shown in Sec. III B, the flow pattern of the cell structure resembles such a central toroidal vortex or a concentric roll, which, due to the geometry considered here, is surrounded by smaller counter-rotating vortices in the corner regions of the square container. Strong regular oscillations are a striking feature of this regime (see Sec. III C). These oscillations are reflections of a mutual

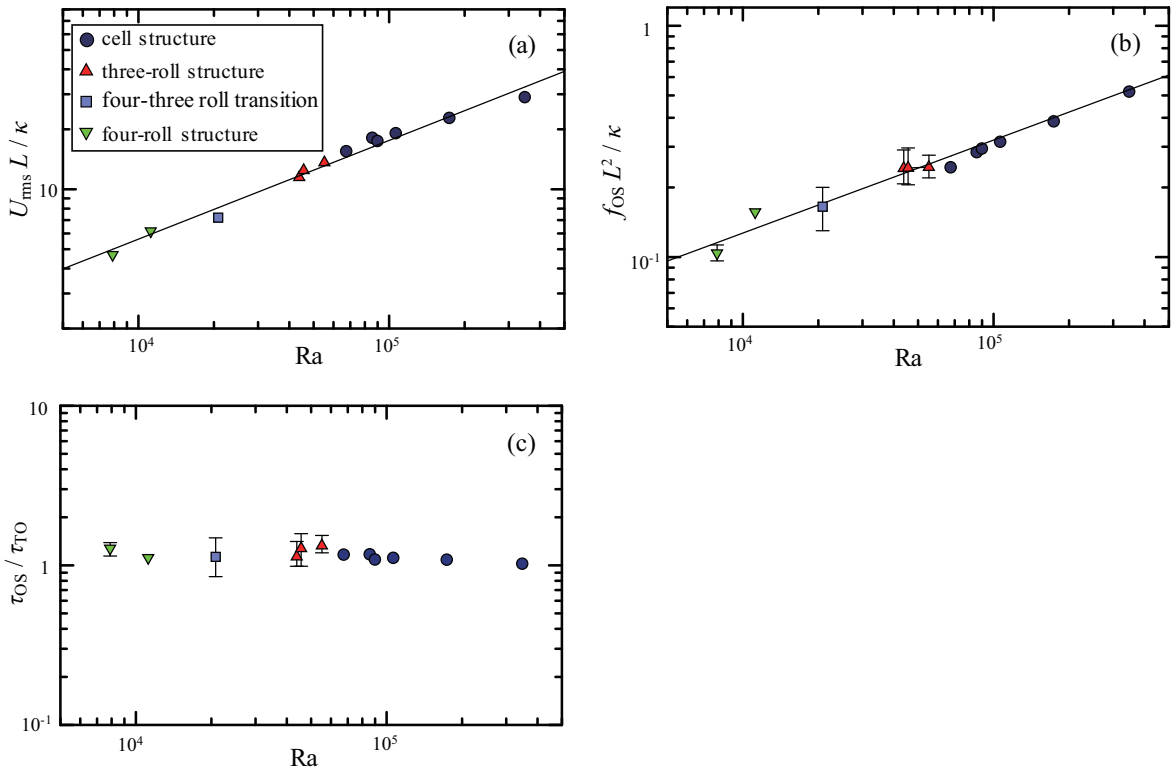

FIG. 10. Plots of (a) the representative flow velocity $U_{\rm rms}$, where the solid line shows the fitting curve given by the least square approximation on the plots, $U_{\rm rms}L/\kappa = 0.059{\rm Ra}^{0.50}$, (b) the frequency of oscillations $f_{\rm OS}$, where the solid line shows the fitting curve on the plots, $f_{\rm OS}L^2/\kappa = 0.039{\rm Ra}^{0.38}$, and (c) the periods of oscillation normalized by the turn-over times $\tau_{\rm TO}$ with respect to Ra

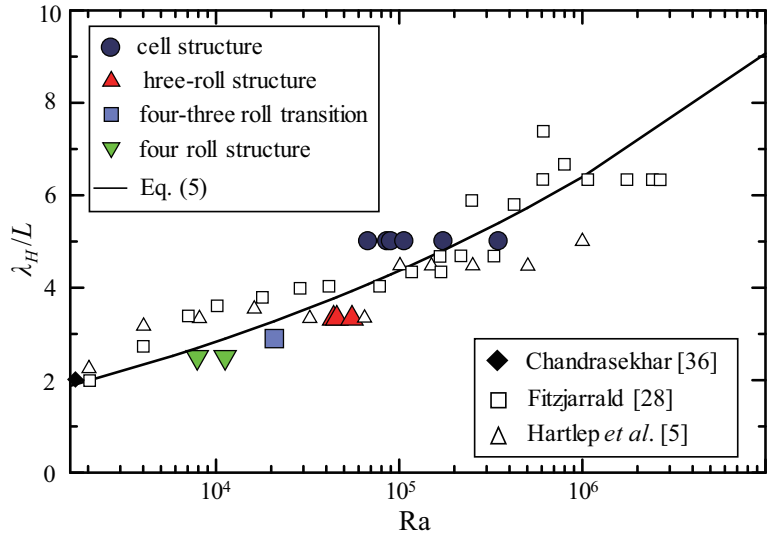

FIG. 11. Horizontal wavelength of the large-scale circulations $\lambda_{\rm H}$ versus Ra, where the solid line indicates relation $\lambda_{\rm H}/L = 1.60{\rm Ra}^{0.12} - 2$; symbols of open triangle and open square are from Hartlep *et al.* [5] and Fitzjarrald [28] obtained in air layers (Pr ~ 0.7) and a symbol black diamond is the critical wavelength $\lambda_{\rm Hc}/L = 2.016$ at ${\rm Ra}_{\rm c} = 1708$ from Chandrasekhar [36].

increase and decrease of the velocities measured in the x- and y-direction on the center lines. A simplified picture in Fig. 8 suggests a periodic elliptical deformation of the concentric roll along the two center lines of the square cross-sectional area. On the basis of the available measurement results, it is ultimately not possible to decide whether such a deformation of an originally axially symmetric structure exists or whether it is even the competition of two interacting double vortices in the x and y direction. In this case the strong oscillations result from the fact that each one of the double rolls dominates alternately during a half-period and the other is strongly damped at the same time. Vasiliev *et al.* —[38] considered the dynamics of the LSC inside a cube. They describe the LSC as a superposition of two-large-scale two-dimensional orthogonal rolls while observable phenomena such as the reorientation of LSC are due to the competition of these two roles.

Fig. 11 represents the variation of the structure size of the characteristic flow patterns with increasing Ra number. Here, the critical wavelength, $\lambda_{\mathrm{Hc}}/L = 2.016$, at the critical Rayleigh number, $\mathrm{Ra_c} = 1708$ [36] is also plotted, which indicates that this point corresponds approximately to the suggested power law. Apart from the fact that the horizontal scale of the coherent structure increases stepwise with increasing Ra number, the assumption that the oscillation period of the structure is comparable to the turn-over time applies to all flow regimes. The flow structure has the feature of traveling-wave convection arising from the oscillatory instability of steady rolls predicted by theory [12], and demonstrated by numerical simulations (e.g., Ref. 14 and 15). With increasing Ra, the structure loses regularity along the rotation axis of the convection rolls. This behavior fits the assumption that the roll-like structures observed in the present study are a remnant of the convection rolls forming at the onset of convection. These structures survived despite exceeding the boundary of the oscillatory instability of the Busse balloon and the development of the thermal turbulence. With approaching a stage at $\mathrm{Ra} \geq 6.0 \times 10^4$ that can be associated with fully developed thermal turbulence, the roll-like coherent structures collapse and a transition to the cell structure occurs.

The wavelengths previously obtained in thermal convection of air layers in the range $\mathrm{Ra} \leq 10^6$ are also plotted in Fig. 11 for comparison. These data were obtained by numerical simulations in a square layer with aspect ratio 10 [5] and experiments in square layers with varying aspect ratios from 2 to 60 [28]. In spite of the difference in the Pr number ($\mathrm{Pr} = 0.7$ for air and $\mathrm{Pr} = 0.03$ for GaInSn), all data fit very well to the curve resulting from Eq. (5). It indicates that this power law is widely applicable for $\mathrm{Pr} \lesssim 1$ in layers having large aspect ratios and covering a wide range of Ra numbers from laminar flows to thermal turbulence. In the present study, we have limitations of experiments, specifically, the range of Ra numbers and the geometry of a vessel.

It is quite an interesting question to ask regarding the further development of the LSC structures at even higher Ra or in convection cells at larger aspect ratio. It is obvious to assume that the horizontal wavelength λ_{H}continues to expand until the entire cell is occupied, that means a single circulation roll is expected to be formed as this is known as typical LSC structure in vessels with $\Gamma \approx 1$ [3, 4]. The occurrence of multiple cellular structures – also called as turbulent superstructures – was recently reported for vessels with much larger aspect ratios than that in the present study [6, 7, 39, 40]. It is reasonable to assume that such multiple cellular structures composed of unit cells having a similar horizontal wavelength as in the cell-like regime found here could occur in vessels of larger aspect ratios at comparable Ra numbers.

V. CONCLUSION

The present study investigates the Rayleigh–B'enard convection inside a liquid metal layer ($\mathrm{Pr} = 0.03$) confined by a flat rectangular vessel having a square horizontal cross section and an aspect ratio of 5. The flow structures in the convection cell were characterized using the ultrasonic velocity profiling (UVP). In a range of moderate Ra numbers, $O(10^4)$–$O(10^5)$, the flow measurements revealed the existence of four different flow regimes. Transitions between these flow regimes occur with increasing Ra number accompanied by a stepwise increase of the horizontal wavelength. Accompanying measurements of the temperature fluctuations indicate that the stage of developed thermal turbulence is reached at Ra numbers $\geq 10^5$.

After the onset of convection the flow forms coherent structures in form of elongated rolls whose axes are aligned parallel to one of the side walls. There is a region in the Ra number – wave number parameter space in which these convection rolls remain stable, called as Busse balloon. A growing Ra number leads first to an exceeding of the stability limit, with the consequence that the convection rolls are subject to oscillatory fluctuations. A further increase in the thermal driving force ultimately produces a fully developed turbulent flow. Oscillatory roll-like structures are observed up to a Ra number of 6.8×10^4. In this parameter range there exist a four-roll and a three-roll regime as well as an unstable intermediate regime in between. Based on previous assumptions, it was not to be expected to observe flow patterns which are dominated by convection rolls. On the other hand, the intrinsically two-dimensional roll structures are disturbed to a considerable extent. Nevertheless, the roll-like structures observed in the present study have their origin in the convection rolls evolving as coherent structures at the onset of convection. The transition from a roll-like structure to a fully three-dimensional cell-like structure occurs around $\mathrm{Ra} = 6.8 \times 10^4$. The cell-like structure appears to be a typical representation of the large-scale circulation (LSC) in thermal turbulence for the geometry

considered here. While the horizontal wavelength of the roller-like structures corresponds approximately to the height of the fluid layer, the wavelength of the cell-like structure is significantly larger.

The scaling law for the spatial wave length λ_H of the coherent structures was derived from the empirical relationships describing the dependency of the oscillation frequency and the representative flow velocity on the Ra number. Our results suggest a relation of $\lambda_H \sim \mathrm{Ra}^{0.12}$, which agrees well also with reported variations of the characteristic size of LSCs in air layers observed for different geometries. This gives reason to assume that this scaling law for the wavelength of coherent structures in thermal convection is valid for different Pr numbers in the range $\mathrm{Pr} \lesssim 1$.

Assumptions can be made concerning the evolution of the coherent flow structures for both higher Ra numbers and aspect ratios. Another incremental increase in horizontal wavelength is expected for a growing Ra number until the convection pattern fills the entire width of the cell. In flat convection cells with a significantly higher aspect ratio, multiple cell structures could emerge, possibly resulting from a periodic sequence of cell-like structures, as observed in this study as a single cell. There is no doubt that the question regarding a potential relation between the cell-like flow structure found in this study and turbulent superstructures is very interesting. Continuing experiments in liquid metal layers are worth to be the subject of further studies.

[1] R. Krishnamurti, J. Fluid Mech. **60**, 285 (1973).
[2] R. Krishnamurti and L. N. Howard, Proc. Natl. Acad. Sci. USA **78**, 1981 (1981).
[3] G. Ahlers, S. Grossmann, and D. Lohse, Rev. Modern Phys. **81**, 503 (2009).
[4] F. Chillà and J. Schumacher, Eur. Phys. J. E. **35**, 58 (2012).
[5] T. Hartlep, A. Tilgner, and F. Busse, Phys. Rev. Lett. **91**, 064501 (2003).
[6] J. von Hardenberg, A. Parodi, G. Passoni, A. Provenzale, and E. A. Spiegel, Phys. Lett. A **327**, 2223 (2008).
[7] M. Emran and J. Schumacher, J. Fluid Mech. **776**, 96 (2015).
[8] J. Bailon-Cuba, M. Emran, and J. Schumacher, J. Fluid Mech. **655**, 152 (2010).
[9] P. J. Sakievich, Y. T. Peet, and R. J. Adrian, Int. J. Heat and Fluid Flow **61**, 183 (2016).
[10] F. H. Busse, Rep. Prog. Phys. **41**, 1929 (1978).
[11] F. H. Busse, J. Fluid Mech. **52**, 97 (1972).
[12] R. M. Clever and F. H. Busse, J. Fluid Mech. **65**, 625 (1974).
[13] R. M. Clever and F. H. Busse, J. Fluid Mech. **176**, 403 (1987).
[14] M. Lappa, *Thermal Convection: Patters, Evolution and Stability* (Wiley, 2010).
[15] A. Nakano, H. Ozoe, and S. W. Churchill, Chem. Eng. J. **71**, 175 (1998).
[16] H. T. Rossby, J. Fluid Mech. **36**, 309 (1969).
[17] T. Takeshita, T. Segawa, J. Glazier, and M. Sano, PhysṘev. Lett. **76**, 1465 (1996).
[18] S. Cioni, S. Ciliberto, and J. Sommeria, J. Fluid Mech. **335**, 111 (1997).
[19] T. Segawa, A. Naert, and M. Sano, Phys. Rev. E **57**, 557 (1998).
[20] S. Horanyi, L. Krebs, and U. Müller, Int. J. Heat & Mass Trans. **42**, 3983 (1999).
[21] U. Burr and U. Müller, Phys. Fluids **13**, 3247 (2001).
[22] J. M. Aurnou and P. Olson, J. Fluid Mech. **430**, 283 (2001).
[23] Y. Takeda, Intl. J. Heat & Fluid Flow **7**, 313 (1986).
[24] in *Ultrasonic Doppler velocity profiler for fluid flow*, Vol. 101, edited by Y. Takeda (Springer, 2012).
[25] T. Mashiko, Y. Tsuji, T. Mizuno, and M. Sano, Phys. Rev. E **69**, 036306 (2004).
[26] Y. Tsuji, T. Mizuno, T. Mashiko, and M. Sano, Phys. Rev. Lett. **94**, 034501 (2005).
[27] T. Yanagisawa, Y. Yamagishi, Y. Hamano, Y. Tasaka, M. Yoshida, K. Yano, and Y. Takeda, Phys. Rev. E **82**, 016320 (2010).
[28] D. E. Fitzjarrald, J. Fluid Mech. **73**, 693 (1976).
[29] Y. Tasaka, K. Igaki, T. Yanagisawa, T. Vogt, T. Zuerner, and S. Eckert, Phys. Rev. E **93**, 043109 (2016).
[30] T. Vogt, W. Ishimi, T. Yanagisawa, Y. Tasaka, A. Sakuraba, and S. Eckert, Phys. Rev. Fluids **3**, 013503 (2018).
[31] Y. Plevachuk, V. Sklyarchuk, S. Eckert, G. Gerbeth, and R. Novakovic, J. Chem. Eng. Data **59**, 757 (2014).
[32] G. K. Batchelor, I. D. Howells, and A. A. Townsend, J. Fluid Mech. **5**, 134 (1959).
[33] S. Lam, x. D. Shang, S.-Q. zhou, and K.-Q. Xia, Phys. Rev. E **65**, 066306 (2002).
[34] T. Yanagisawa, Y. Hamano, T. Miyagoshi, Y. Yamagishi, Y. Tasaka, and Y. Takeda, Phys. Rev. E **88**, 063020 (2013).
[35] J. Scheel and J. Schumacher, J. Fluid Mech. **802**, 147 (2016).
[36] S. Chandrasekhar, *Hydrodynamic and Hydromagnetic Stability* (Oxford University Press, 1961).
[37] F. Hébert, R. Hufschnid, J. Scheel, and G. Ahlers, Phys. Rev. E **81**, 046318 (2010).
[38] A. Vasiliev, P. Frick, A. Kumar, R. Stepanov, A. Sukhanovskii, and M. Verma, ArXiv , 1805.06718v1[physics.flu.
[39] R. J. A. M. Stevens, A. Blass, X. Zhu, R. Verzico, and D. Lohse, Phys. Rev. Fluids **3**, 041501 (2018).
[40] A. Pandey, J. D. Scheel, and J. Schumacher, Nat. Commun. **9** (2018).